Palaeo-earthquake Magnitudes and Current Deformation on the Dzhungarian Fault, N. Tien Shan, and Implications for the Rupture Processes of Intraplate Strike-slip Faults

Chia-Hsin (Wendy) Tsai[1], Richard T. Walker[1], Simon Daout[1], Kanatbek Abdrakhmatov[2], Aidyn Mukambayev[3], Christoph Grützner[4], Ed Rhodes[5]

[1] Department of Earth Sciences, University of Oxford, UK, [2] Institute of Seismology, National Academy of Sciences, Kyrgyz Republic, [3] Data Center of the Institute of Geophysical Researches, Kazakhstan, [4] Institute of Geological Sciences, Friedrich Schiller University Jena, Germany, [5] Department of Geography, University of Sheffield, UK

COMET

1. INTRODUCTION

Long-term and present-day crustal deformation in the northern Tien Shan is poorly known, but is a key to understanding the mode of lithospheric deformation deep within the continental interiors, as well as the hazards posed by the slow-moving intraplate faults. Here we focus on the NW-SE striking Dzhungarian fault (DZF) and the E-W striking Lepsy fault (LPF), which are large oblique strike-slip faults bounding the Dzhungarian Alatau, northern Tien Shan. Two large historical earthquakes in ~1716 and 1812 (Mw 8) were recorded in this region, and clear fault traces as well as scarps are visible from satellite images. However, their slip rates, mode of deformation, expected earthquake magnitudes and recurrence interval have not been studied in details. A previous study shows offsets of 8.2-13.8 m were found along the 120 km LPF in ~400yrBP, indicating a magnitude in the range Mw 7.5-8.2 (Campbell, et al., 2015). The slip to length ratio for the LPF is unusually high, suggesting either that faults in this region are capable of generating very large earthquakes for a given fault length, or that the rupture length is underestimated. By studying the palaeo-earthquakes along the neighboring DZF from the surface ruptures, we could have more insights into the rupture processes and the scaling of earthquakes in this region. InSAR time-series analysis is also applied to reveal the deformation across the DZF for understanding the current crustal strain.

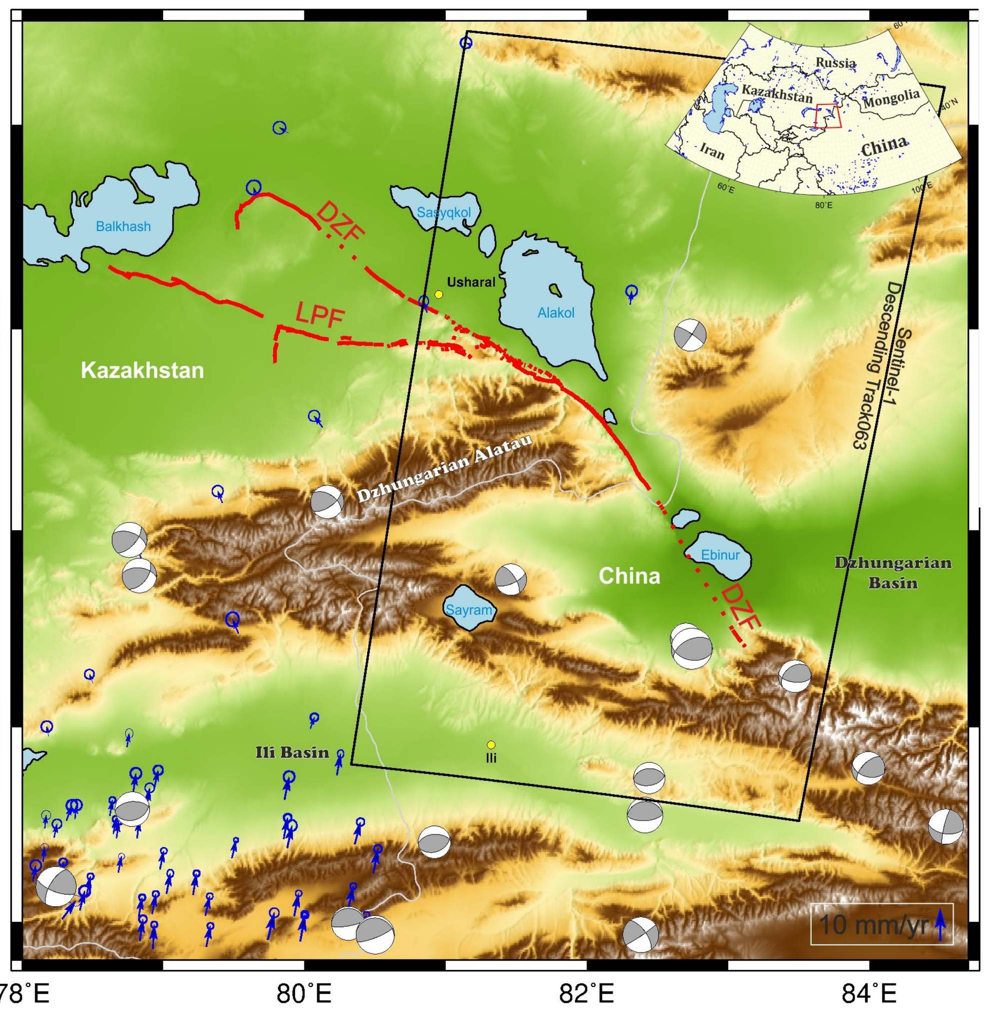

↑Figure 1. The topographic map of northern Tien Shan.

2. Mapping

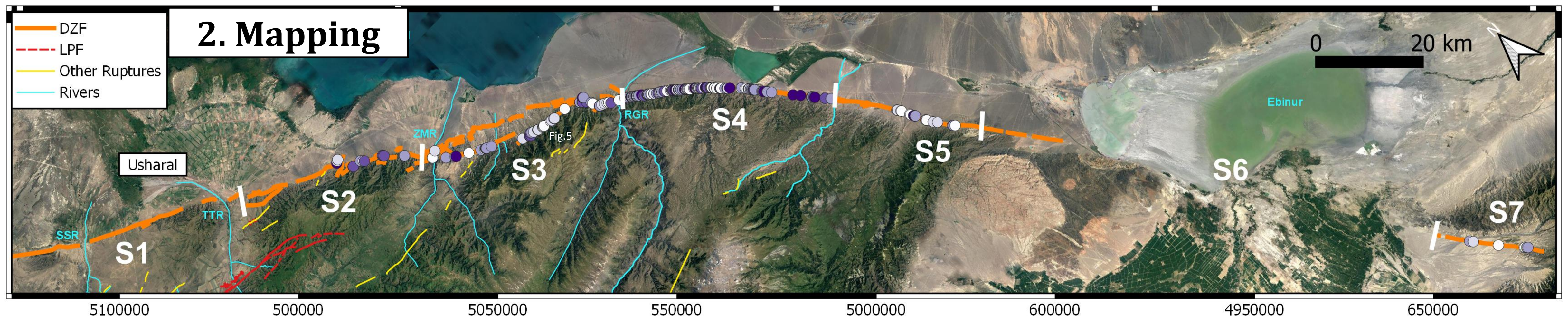

↑ Figure.2. Mapping of the DZF. Using a combination of high-resolution digital elevation models (DEMs) and ortho-rectified photos, we mapped out the fault traces and identified every surface ruptures. The 237 purple points are the locations where lateral offset could be found with the darker ones indicating the smaller amount of offset. We further separate the DZF into 7 sections according to the strike directions and the rupture types. Note that a few ruptures could be found inside or at the northern edge of Dzhungarian Alatau as well.

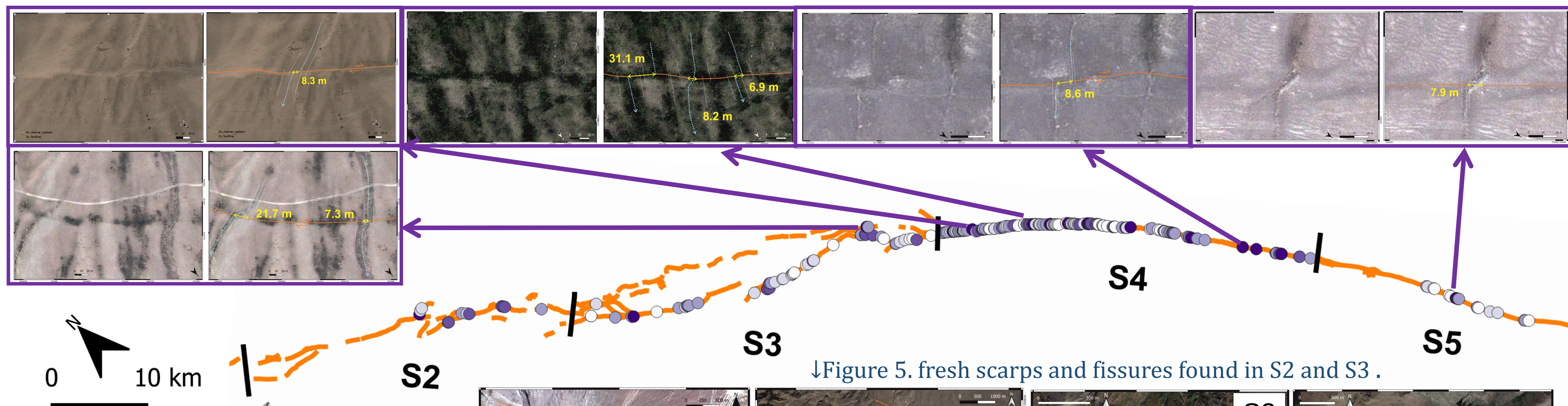

↑Figure 3. The smallest amount of displacement found along the DZF (S2-5). The purple points are the locations of discovered lateral offset. The darkest color indicates the offset is less than 15 m.

↓Figure 5. fresh scarps and fissures found in S2 and S3 .

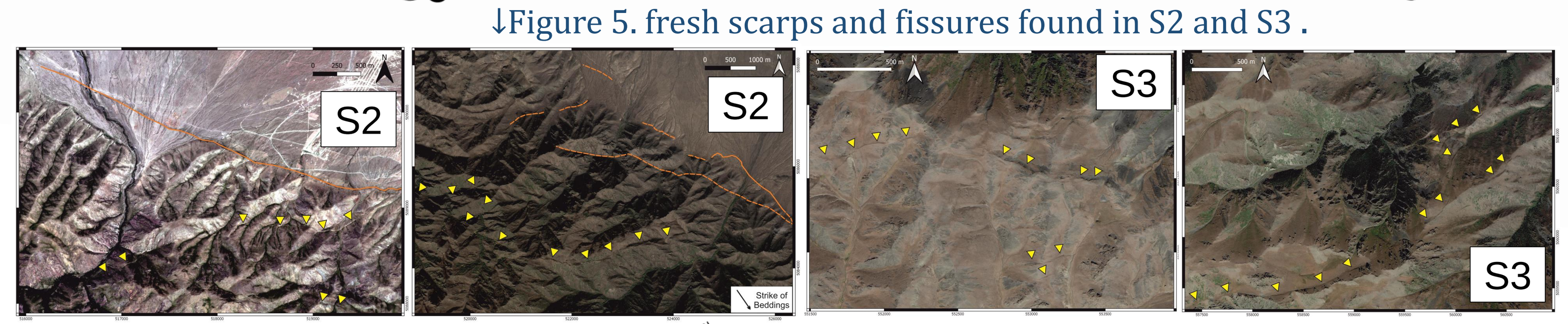

3. Geomorphology and Total Slip Estimation

The fresh ruptures only appear south of City Usharal, from S2 to S5 (with a few in S7). Fault traces could hardly be found in S6. The southern DZF (S4,5) is nearly pure strike-slip and the middle DZF (S3) has 2 branches as the strike gradually changes by ~18°. Section 3 is a typical slip-partioning section with the eastern branch dominated by reverse component but the western one mostly pure strike-slip. The northern DZF (S2) has both lateral and reverse components (fig. 6). In S4 and S5, the smallest offset could be found is 6.9-8.6 m, indicating the amount of total slip of the last event.

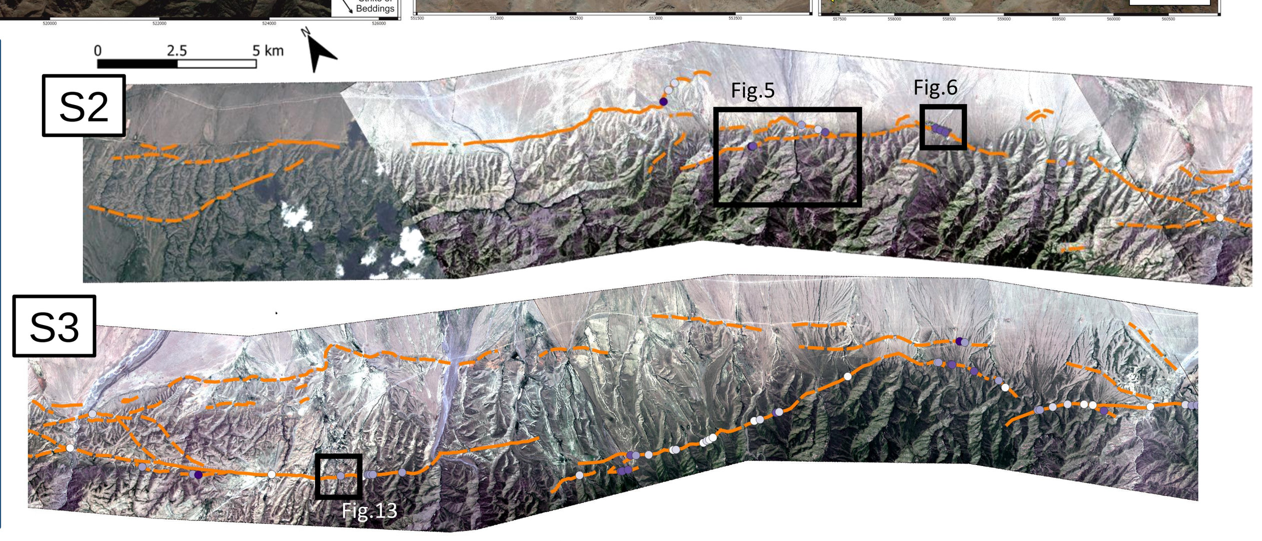

↑ Figure 4. Pleiades images of S2 and S3 with DZF fault traces mapped. S2 has lots of discontinuous fault traces and fresh scarps. S3 has fresh ruptures concentrated on the western branch.

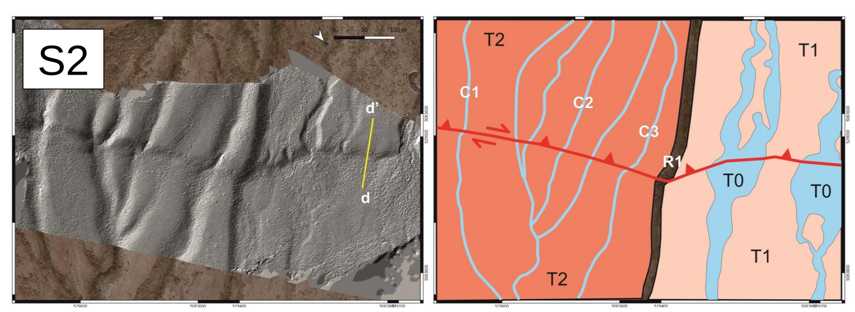

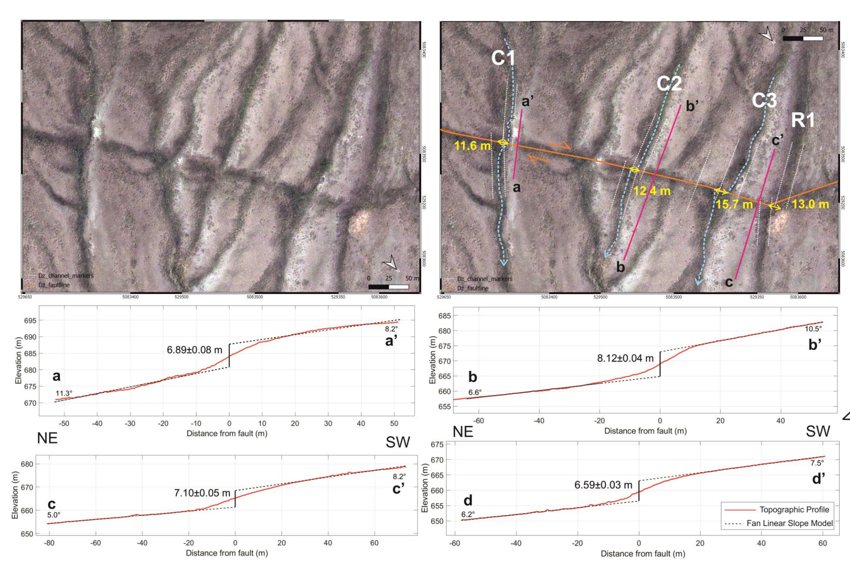

↑Figure 6. The evidence of both reverse and strike-slip component found at S2. This location is also at the eastern extension of LPF (fig. 2). The lateral offset here is 12~16 m, the vertical offset is 6~8 m. The ratio of lateral to vertical slip is ~ 1.7:1, which helps to estimate the net slip (fig.7).

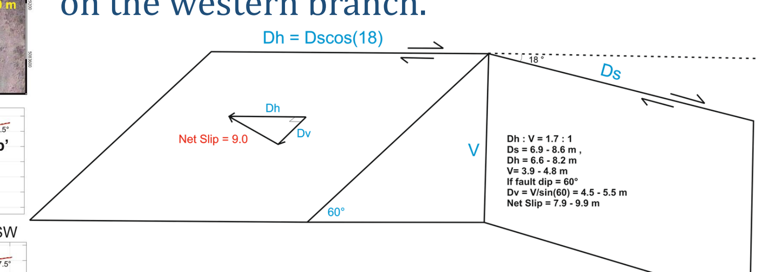

↑ Figure 7. Simplified geometry of DZF and the estimation of total slip in S2.

4. Magnitudes (Mw) Estimation

Considering the widely distribution of fresh ruptures from S2-5, it is likely that the last event has ruptured northern part of DZF as well. By assuming the same lateral slip vector and a dipping angle of 60°, the total slip in the northern DZF (S2) could be up to 7.9-9.9 m (fig. 7). Such amount of total slip is similar to the one found along the LPF, suggesting the possibility for them to rupture together. Considering different scenarios of rupture length and assuming the seismogenic depth to be 15-30 km, the possible moment magnitude of the last event is 7.7 – 8.3 (table1). The slip to length ratio is 2.9-8.8 x 10^{-5}, which is slightly higher than normal cases.

↓ Table 1. Moment magnitude estimation from different rupture scenarios and their corresponding fault parameters.

Rupture Scenario	Rupture Length	Total Slip	Dipping Angle	Depth	Magnitude (Mw)
DZF S2-S5	140 km	6.9 – 9.9 m	30 - 90°	15 -30 km	7.7 - 8.0
LPF + DZF S2	155 km	8.2 – 13.8 m	50 - 60°	15 -30 km	7.8 - 8.2
LPF + DZF (S2-S5)	260 km	6.9 – 13.8 m	50 - 90°	15 -30 km	7.9 – 8.3

5. InSAR Data Processing

This study presents a 5-year time-line InSAR time series from Satellite Sentinel-1 descending track 063 (fig. 1). We process 370 interferograms with the New Small Baselines Subset (NSBAS) processing chain (Doin et al., 2011, Grandin 2015). The extreme seasonal variations in climate and abrupt changes in soil moisture produce severe unwrapping difficulties (fig. 8). We proceed to a series of corrections on the wrapped phase to help for unwrapping (the chart-flow). We put specific focus on moisture-related seasonal deformation signals that we extract with a Principal Component Analysis (PCA) (fig. 9). Joint correction of atmospheric delays based on ERA-5 models and a linear ramp is further applied (fig. 10) before the time series analysis and the extraction of the average Line of Sight (LOS) velocity map from 2014 to 2019 (fig. 11 & 12).

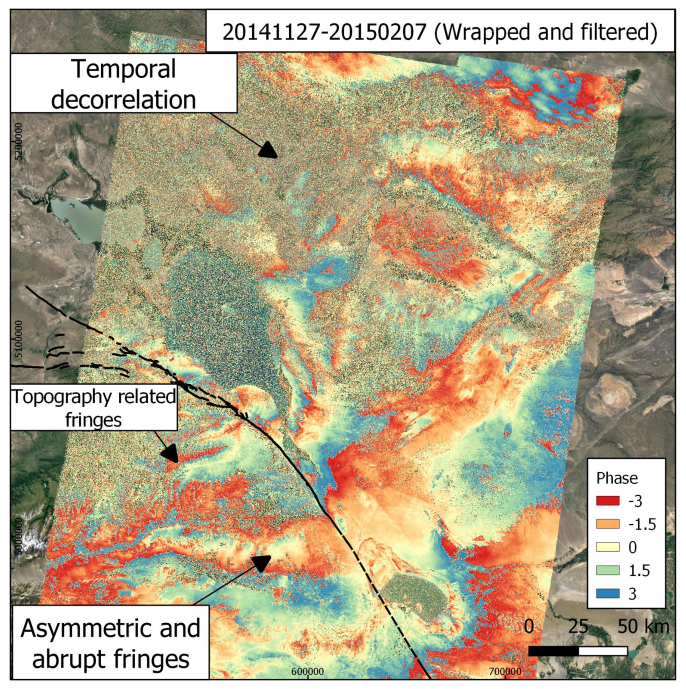

←Figure 8. Example of wrapped and filtered interferogram showing the different challenges in this mountainous and vegetated area: 1) topography-correlated fringes due to stratified delays, 2) local patterns of deformation altering the phase continuity, 3) temporal deccorrelation due to abrupt changes of soil properties. The alluvial fans and agricultural fields trigger asymmetric and abrupt fringes, which leads to major unwrapping errors.

- Step 1: Interferogram generation
- Step 2: Empirical phase-elevation correction on wrapped phase
- Step 3: Computing the colinearity on wrapped phase
- Step 4: Filtering on wrapped phase and unwrapping
- Step 5: Implementing principle component analysis (PCA) on correctly unwrapped images
- Step 6: Correction of signals on wrapped phase by the PCA model
- Step 7: Re-filtering on wrapped phase and re-unwrapping
- Step 8: Adding back atmospheric and PCA signals from step 2 and step 6
- Step 9: Correction of ramp and atmospheric signal by ERA-5
- Step 10: Time-series analysis and LOS velocity computation

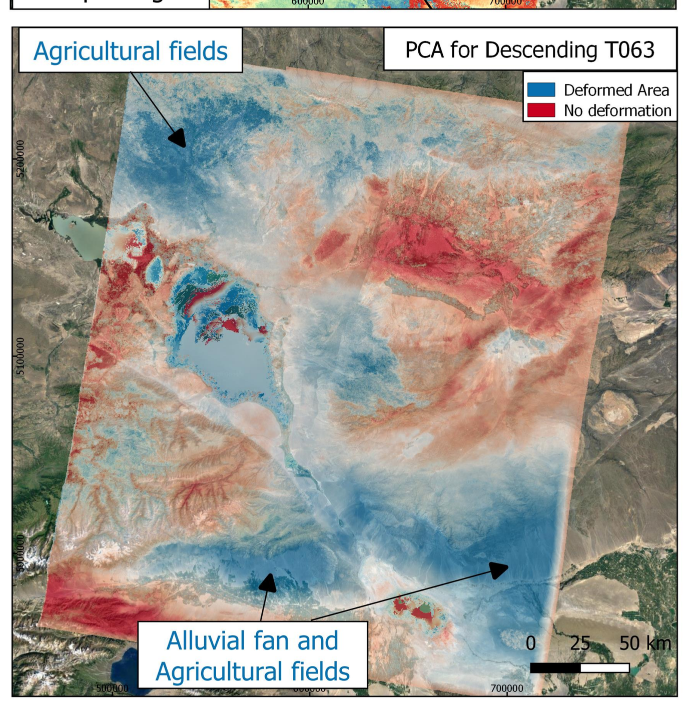

↑Figure 9. We extract a deformation template by PCA (blue patters are deformation areas within the alluvial fans and agricultural fields). Unwrapping proceeds spatially with a path based on the colinearity. The template is used to artificially decrease the colinearity and avoid difficult areas. We also removed the template from the original interferograms to help for unwrapping and re-introduce it afterwards.

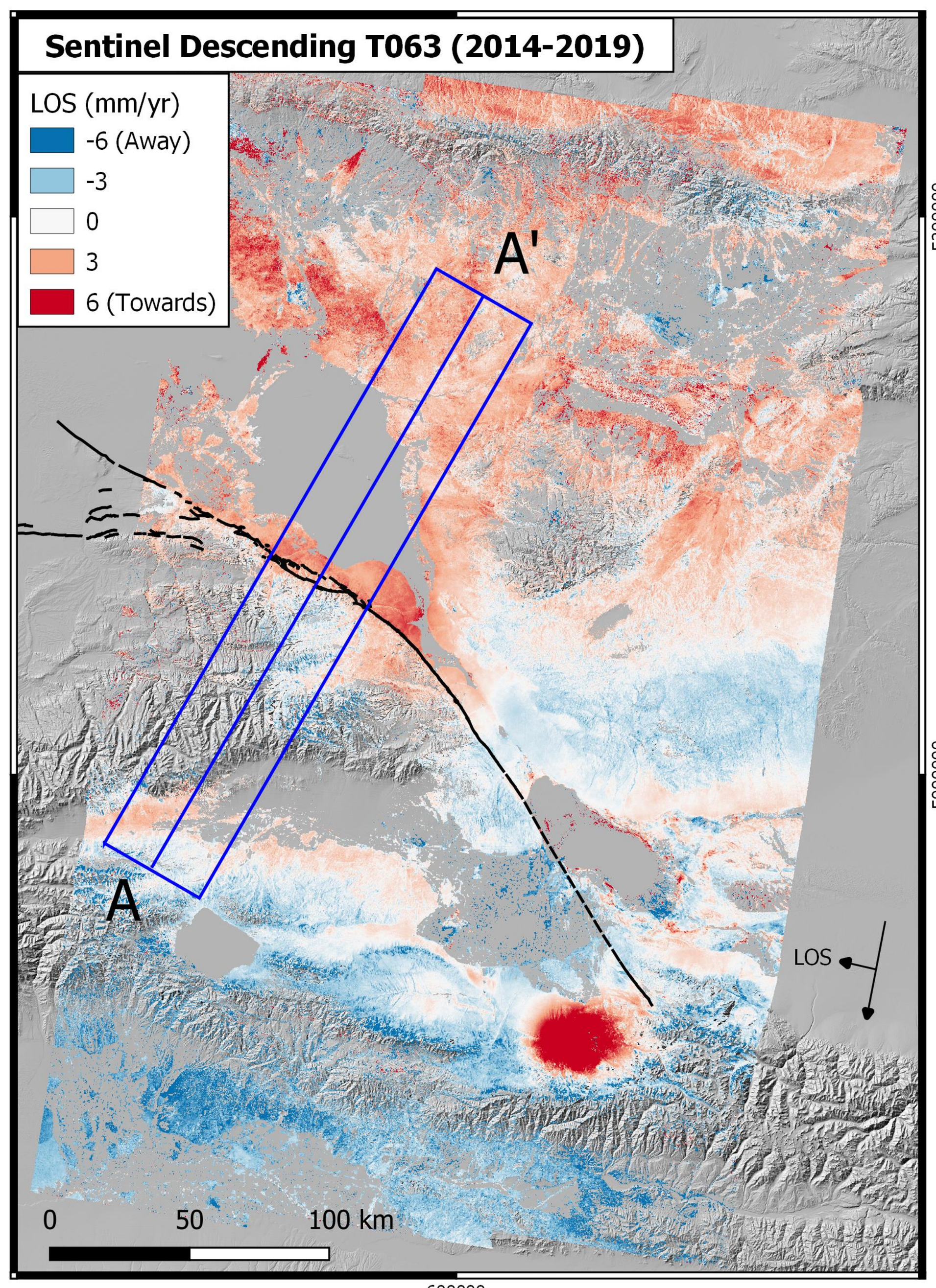

↑Figure 11. LOS velocity map superimposed on shaded elevation with location of the profile A-A' centred on the right-lateral DZF. (The uplift in the southeast is a Mw 6.3 event on 8th August 2017 as labeled in Fig. 1.)

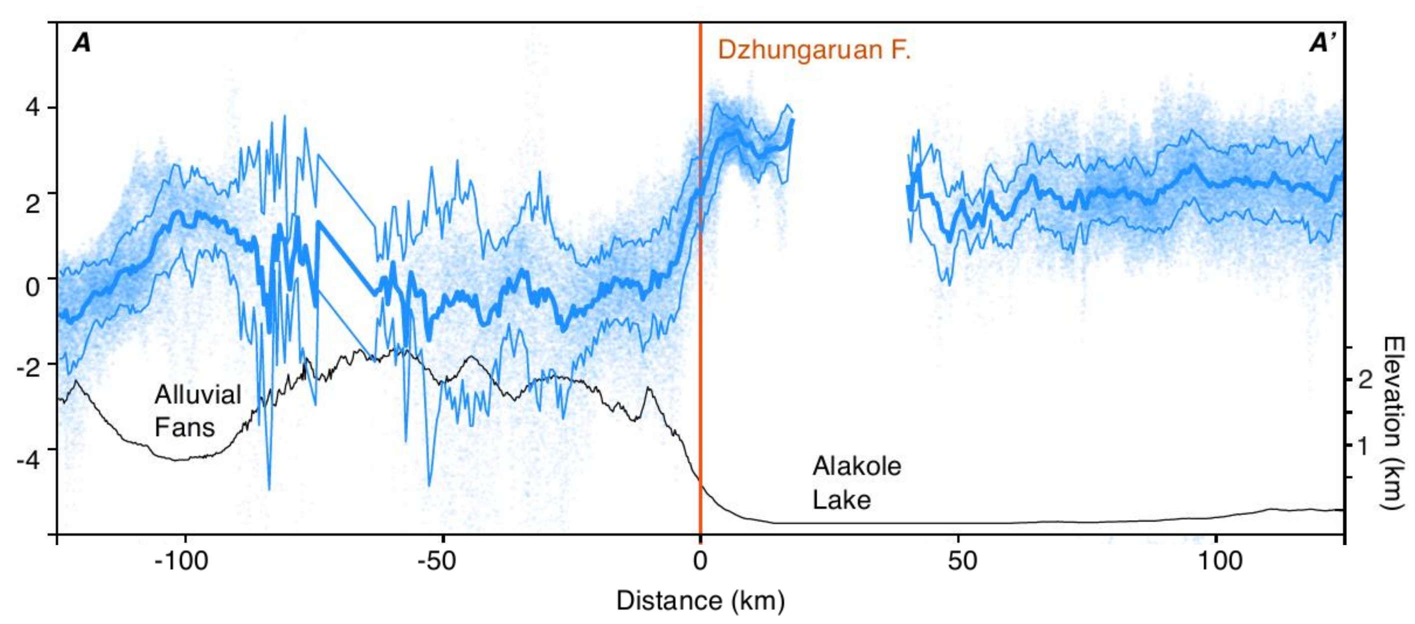

← Figure 12. LOS velocity and elevation profile AA'. The tangent-like curve indicates a current LOS velocity gradient of deformation across the fault ~ 2 mm/yr across the fault due the inter-seismic loading along the fault.

→Figure 10. The phase correlation is good in the joint correction of atmospheric delay and linear ramp.

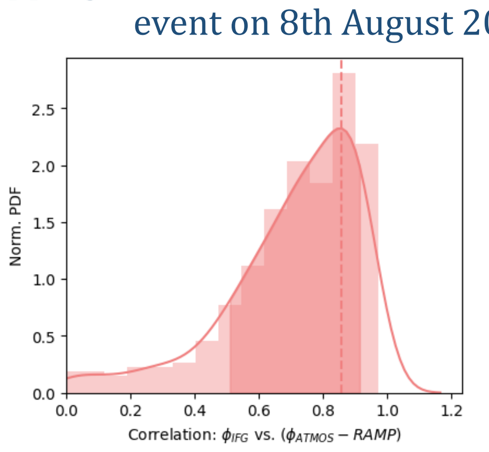

6. Slip Rate

Campbell et al. (2013) presents a Quaternary long-term lateral slip rate of 2.2 ± 0.8 mm/yr from the ~26 ka IRSL samples collected at a ~50 m offset river bank at S4. We also gets a lateral slip rate of 1.7 ± 0.5 mm/yr from the ~12 ka IRSL sample collected at a ~19 m offset gulley at western branch of S3 (fig. 5 &13). This rate should be less than the total slip rate since the slip partitioned in S3. The current slip rate of DZF is still needed to be further derived from the LOS velocity.

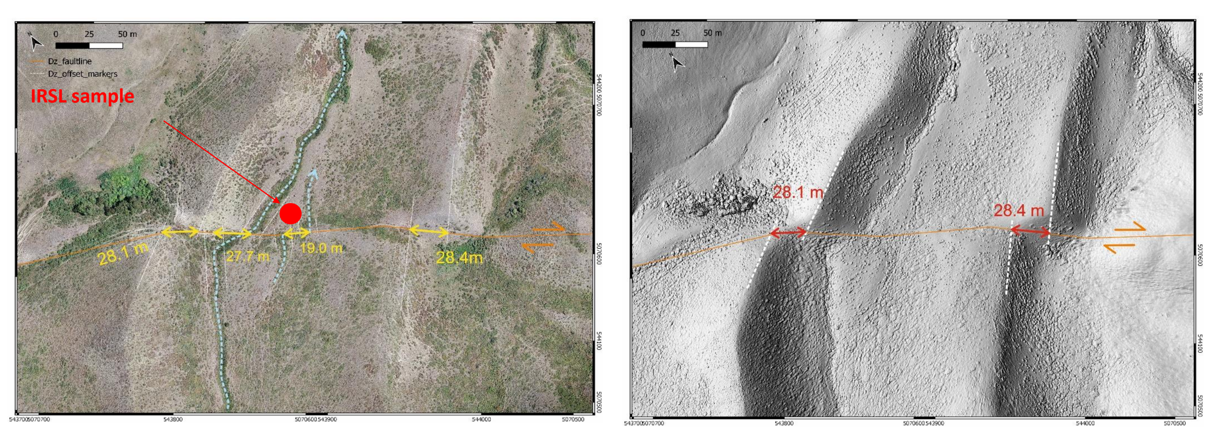

←Figure 13. The surface displacement and the IRSL sample collected at the western branch of S3.

References:

- Campbell, G. E. et al. (2015), Great earthquakes in low strain rate continental interiors: An example from SE Kazakhstan, J. Geophys. Res. Solid Earth, 120, 5507–5534, doi:10.1002/2015JB011925.
- Campbell, G. E. et al. (2013), The Dzhungarian fault: Late Quaternary tectonics and slip rate of a major right-lateral strike-slip fault in the northern Tien Shan region, J. Geophys. Res. Solid Earth, 118, 5681–5698, doi:10.1002/jgrb.50367.
- Doin, M.-P. et al. (2011), Presentation of the small baseline NSBAS Processing chain on a case example : The etna deformation monitoring from 2003 to 2010 using Envisat data. Proc. esaFringe.
- Grandin, R. (2015) Interferometric Processing of SLC Sentinel-1 TOPS Data. Fringe 2015 36.